iScience

CellPress
OPEN ACCESS

Article

Microbiota-derived imidazole propionate inhibits type 2 diabetic skin wound healing by targeting SPNS2-mediated S1P transport

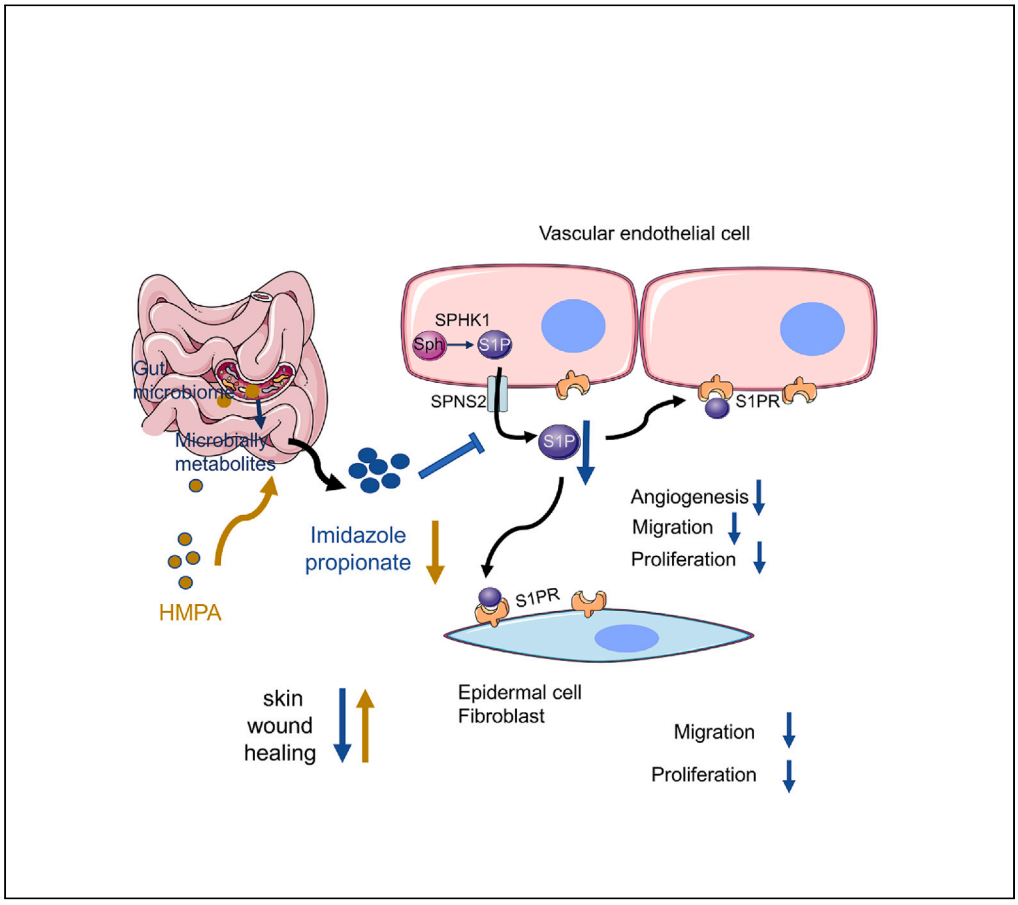

Shaoting Zheng, Hongqi Wang, Jingxia Han, Xintong Dai, Ying Lv, Tao Sun, Huijuan Liu

tao.sun@nankai.edu.cn (T.S.)
liuhuijuanxyz@163.com (H.L.)

Highlights

ImP inhibits angiogenesis during wound healing

ImP inhibits SPNS2-mediated S1P secretion and Rho signaling pathway activation

HMPA reduces ImP levels and promotes the wound healing process in T2DM mice

Zheng et al., iScience 26, 108092
November 17, 2023
https://doi.org/10.1016/j.isci.2023.108092

iScience

CellPress
OPEN ACCESS

Article

Microbiota-derived imidazole propionate inhibits type 2 diabetic skin wound healing by targeting SPNS2-mediated S1P transport

Shaoting Zheng,[1,2,3] Hongqi Wang,[1,2,3] Jingxia Han,[1] Xintong Dai,[1] Ying Lv,[1] Tao Sun,[1,2,*] and Huijuan Liu[1,2,4,*]

SUMMARY

Imidazole propionate (ImP) is a recently discovered metabolite of T2DM-related gut microbiota. The effect of ImP on T2DM wound healing has not been studied yet. In this research, the changes of ImP-producing bacteria on the skin are firstly evaluated. 16sRNA sequencing results showed that the abundance of ImP-producing bacteria-Streptococcus in the intestine and skin of T2DM mice is significantly increased. Animal experiments show that ImP can inhibit the process of wound healing and inhibit the formation of blood vessels in the process of wound healing. Molecular mechanism research results show that ImP can inhibit S1P secretion mediated by SPNS2, and inhibit the activation of Rho signaling pathway, thereby affecting the angiogenesis process of HUVEC cells. This work also provides a potential drug HMPA that promotes T2DM wound healing.

INTRODUCTION

Type 2 diabetes mellitus (T2DM) is a common metabolic disease.[1] Approximately 463 million patients with diabetes aged 20–79 have been recorded.[2] Patients with T2DM are prone to various complications, including skin damage and delayed wound healing.[3,4] Poor skin damage repair in T2DM may result in chronic ulceration[3] and subsequent amputation of lower limbs.[5] In patients with diabetes, the incidence of diabetic foot ulcer is 4%–10%,[6] which is the main reason for the hospitalization of patients with diabetes.[7] The inhibition of angiogenesis by vascular endothelial cell damage is one of the important reasons for slow wound healing in patients with T2DM.[8] Elucidating the molecular mechanism of T2DM vascular endothelial cell damage is of great significance to the treatment of T2DM-related vascular degeneration and wound healing.

The intestinal bacterial gut microbiota, as an internal environmental factor, is closely related to the occurrence and development of T2DM.[9] The intestinal bacterial gut microbiota participates in T2DM through a variety of different pathways, such as short-chain fatty acid metabolism pathway,[10] lipopolysaccharide pathway, branched chain amino acid metabolism pathway.[11,12] Imidazole propionate (ImP) was the first T2DM-related metabolite reported by Ara Koh.[13] Patients with T2DM have high concentrations of ImP in their portal veins and peripheral blood. ImP is produced by the T2DM-associated microbiome through the metabolism of histidine, which induces impaired glucose metabolism by activating p38γ-mTOR1-S6K1 signaling. The effects of ImP as a newly discovered metabolite of intestinal bacterial gut microbiota on skin tissue damage and repair have not been explored.

S1P is a sphingolipid metabolite with a wide range of biological activities. S1P is produced by sphingosine kinase-1 and -2.[14] S1P produced in the cells is transported out of the cells (inside-out), and then combined with S1P-specific G protein-coupled receptors (S1PRs) to regulate cell growth, angiogenesis, lymphangiogenesis, and endothelial and epithelial barrier functions.[15,16] S1P regulates angiogenesis by binding S1PR1 and S1PR3 on vascular endothelial cells and inducing them to form capillary networks.[17] The main sources of S1P *in vivo* are hematopoietic and vascular endothelial cells. The release of S1P in hematopoietic cells is mainly through the ABC transporters, whereas the release of S1P in vascular endothelial cells is through spinster homolog 2 (SPNS2).[18,19] S1P plays an important role in angiogenesis, a key process in wound healing. So this work focused on whether ImP inhibiting wound healing through affecting the S1P signaling pathway.

In this study, *in vivo* and *in vitro* experiments and proteomics methods were adopted to evaluate the effects of ImP on T2DM wound healing, vascular endothelial cell function, and angiogenesis. Moreover, whether ImP affects the function of vascular endothelial cells through the S1P pathway was studied, and the effect of the small-molecule HPMA, which can regulate gut microbiota discovered in our previous work, on T2DM skin wound healing was evaluated.

[1]State Key Laboratory of Medicinal Chemical Biology and College of Pharmacy, Nankai University, Tianjin, China
[2]Tianjin International Joint Academy of Biomedicine, Tianjin, China
[3]These authors contributed equally
[4]Lead contact
*Correspondence: tao.sun@nankai.edu.cn (T.S.), liuhuijuanxyz@163.com (H.L.)
https://doi.org/10.1016/j.isci.2023.108092

RESULTS

Imidazole propionate inhibits the skin wound healing in normal mice and type 2 diabetes mellitus mice

The differences in gut microbiota and skin gut microbiota between normal and T2DM mice were firstly detected by the 16S rRNA method. The results showed that the composition of the intestinal and skin gut microbiota of the two groups was obviously different at the genus level (Figures 1A and 1B). Compared with the T2DM group, the Normal group had a higher number of genera (21 species) with abundance >1%. The T2DM group only had 15 species with abundance >1%. The abundance of ImP-producing bacterium *Streptococcus* in the T2DM group was significantly higher. The test results of the skin gut microbiota showed that the abundance of *Streptococcus* in the T2DM group was significantly higher than that of the normal group ($p < 0.05$; Figure 1C). Meanwhile, we examined the metabolic indexes of fasting blood glucose (FSG), total cholesterol (TC), triglyceride (TG), and low-density lipoprotein cholesterol (LDL-C) in T2DM mice. The results showed that there was a significant difference in the metabolic data between the normal and T2DM mice, indicating that the establishment of the T2DM model was successful (Figure S1).

A normal mouse skin wound model was established to evaluate the effect of ImP on skin tissue wound healing. The results showed that compared with the control group, the wound healing rate of the mice in the ImP treatment group was slowed and dose-dependent (Figure 1D). On the 9th day, the wounds in the control group were almost completely healed, whereas the wounds in the ImP group were still unhealed. In this work, a T2DM wound model was also established to evaluate the effect of ImP. The wound healing rate of the T2DM group was slower overall than the normal control group. The rate of skin wound healing in the T2DM mice treated with ImP was slower than the T2DM control group, and the inflammatory response at the wound was obvious (Figure 1E). The statistics of wound healing rate were shown in Figures 1F and 1G. In addition, a pseudo germfree T2DM model (PGF-T2DM; Figure 1H) was established to evaluate the effect of gut microbiota and ImP on wound healing. The experimental results showed that the wound healing rate of the PGF-T2DM model was faster than that of the T2DM control group, indicating that the gut microbiota can influence the wound healing rate. The wound healing rate of the ImP-treated PGF-T2DM group was slower than that of the PGF-T2DM model group (Figures 1I–1K).

Imidazole propionate affects the tissue morphology and collagen production of the wounds

Figure 2A showed the results of H&E staining of the skin tissues of mice in the normal and T2DM groups on day 9 after the wounds were inflicted. The skin tissues of the wounds in the normal group grew well with complete epidermal layers, and the wounds were almost completely healed. By contrast, in the ImP-treated group, especially the high-dose group, the epidermal tissues grew slowly with a large degree of inflammatory cell infiltration, and the scabs at the wounds did not fall off. Complete epidermal tissues at the wound did not form in the T2DM group unlike in the normal group, and the fibrous tissues of the dermis was sparse. In the T2DM-ImP group, large areas of the skin tissues at the wounds were unhealed, scabs were still be found at the wounds, the growth of granulation tissues was slow, and macrophages and neutrophils were infiltrated. After Masson staining, collagen fibers were blue; muscle fibers, cytoplasm, cellulose, keratin and red blood cells were red; and nuclei were blue-brown. As shown in Figure 2B, blue collagen fibers formed in each group on day 9 after wounding. In the normal control group, blue collagen fibers were arranged tightly and regularly, whereas blue collagen fibers in the ImP-treated group were lower in number and sparse. Few and sparce blue collagen fibers were observed in the T2DM control group, and almost no collagen was produced in the wounds in the T2DM-ImP group. The skin tissue healing in the PGF-T2DM group was better than that in the T2DM group, and the epidermal tissue growth was relatively complete. Wound healing in the PGF-T2DM-ImP group was slow and the epidermal tissue did not form completely (Figure 2C). Collagen production in the control group of the PGF-T2DM group was higher than that in the T2DM control group and lower than that in the normal control group. Collagen production in the PGF-T2DM-ImP group was significantly reduced (Figure 2D). These results indicated that ImP can prolong the inflammatory reactions in wounds, inhibit the growth of collagen tissues, and reduce the speed of wound healing.

Imidazole propionate can inhibit the expression of Ki67, vimentin, and CD31

To further confirm the influence of ImP, immunohistochemical experiments were used to detect protein markers related to wound healing. Ki67 is an important protein indicating the state of cell proliferation.[20] The results showed that Ki67 staining was weaker in the wound tissues of the ImP treatment group compared with the control group (Figure 2E). In wound healing, the migration of fibroblasts and keratinocytes play important roles.[21,22] Therefore, the expression of vimentin related to cell migration was evaluated. The experimental results showed that the expression of vimentin in the skin wound tissues of mice decreased after ImP treatment. CD31 was associated with endothelial cell angiogenesis.[23] The rate of CD31-positive cells in the skin wound tissues of the ImP group significantly reduced and was dose dependent (Figures 2E and 2F). The above results further indicated that ImP can inhibit skin wound healing.

Imidazole propionate mainly inhibits the function of the vascular endothelial cell HUVEC

The influence of ImP on HUVEC, NIH-3T3, and HaCaT cell functions related to skin wound healing was further tested. The effects of different concentrations of ImP on the viability of the cells were studied. The results were presented in Figure 3A. The viability of HUVEC cells decreased with the increasing concentration of ImP in a dose-dependent manner. However, ImP showed no obvious effect on the viability of NIH-3T3 and HaCaT cells. In addition, we investigated the temporal gradient cytotoxicity effect of ImP on HUVEC cells and found that 0 nM-1 μM concentrations of ImP were non-toxic to cells over different temporal gradients (24–72 h) (Figure S2). The results of tube formation experiments showed that the number of nodes formed by HUVEC cells in the ImP-treated group were lower than those in the control group

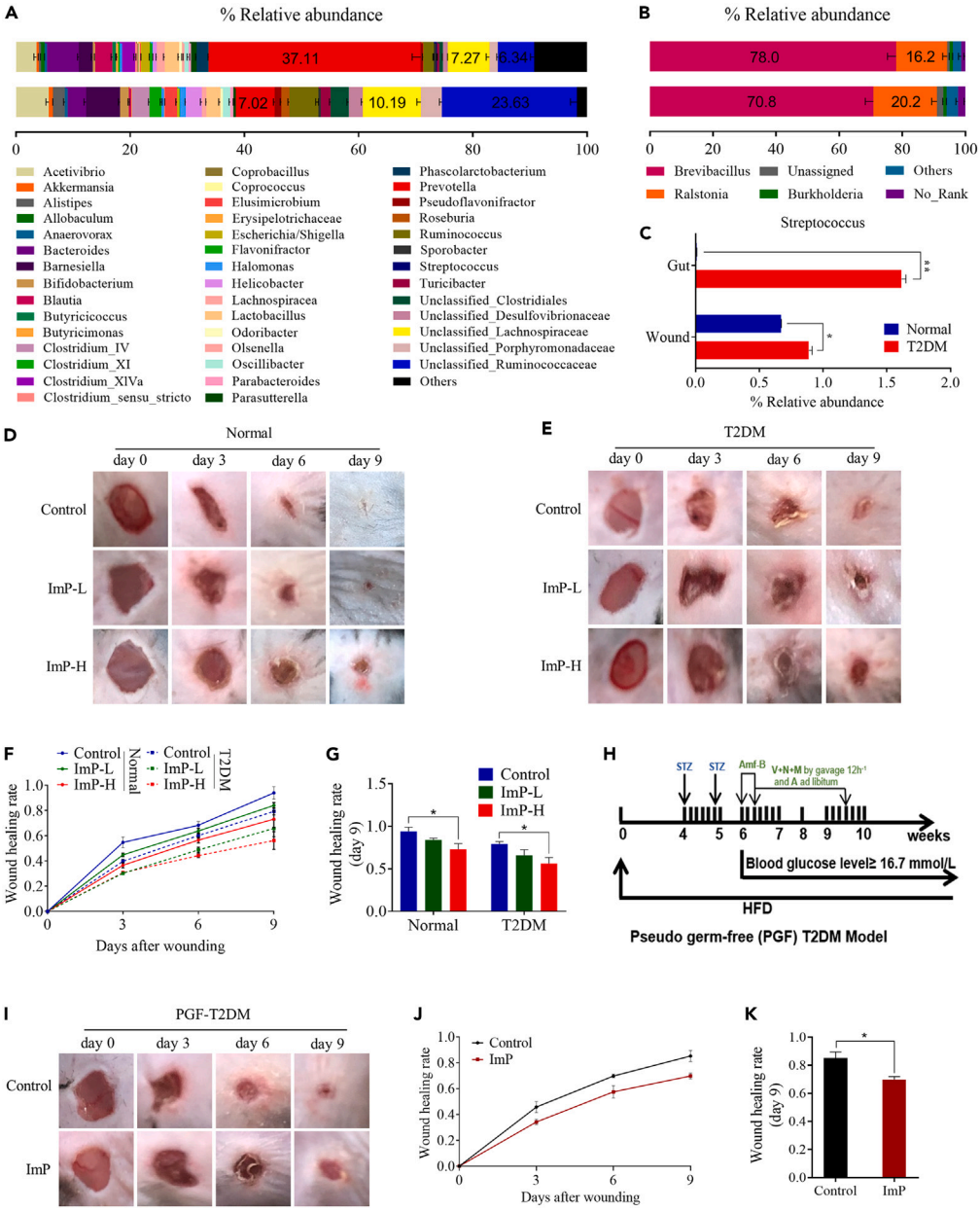

Figure 1. Imidazole propionate (ImP) can inhibit skin wound healing in normal, T2DM, and PGF-T2DM mice

(A) Detection of the difference in genus abundance of the gut microbiota between normal and T2DM mice through the 16S rRNA sequencing (n = 6).

(B) Difference in the genus level of skin gut microbiota between normal and T2DM mice (n = 6).

(C) Difference in the abundance of Streptococcus in the intestines and skin wounds between the normal and T2DM groups.

(D) The effect of ImP on skin wound healing in normal mice (n = 6). ImP-L: 700 nM, ImP-H: 1.5 μM, dermal topical administration.

(E) The effect of ImP on skin wound healing in T2DM mice (n = 6). ImP-L: 700 nM, ImP-H: 1.5 μM, dermal topical administration.

(F) The skin wound healing rate-time curves of ImP-treated normal and T2DM mice.

(G) Statistics of wound healing rate in the skin tissues of ImP-treated normal and T2DM mice (9 Days after wounding).

(H) Schematic diagram of pseudo germfree mice-T2DM (PGF-T2DM) model establishment.

(I) The effect of ImP (2 mg/mL, intragastric administration) on the wound healing of skin tissues in the PGF-T2DM mice (n = 6).

(J) Skin wound healing rate-time curves of ImP-treated PGF-T2DM mice.

(K) Statistical graph of wound healing rate of skin tissues in the ImP-treated PGF-T2DM mice (9 Days after wounding). Data were expressed as mean ± SD (*$p < 0.05$, **$p < 0.01$).

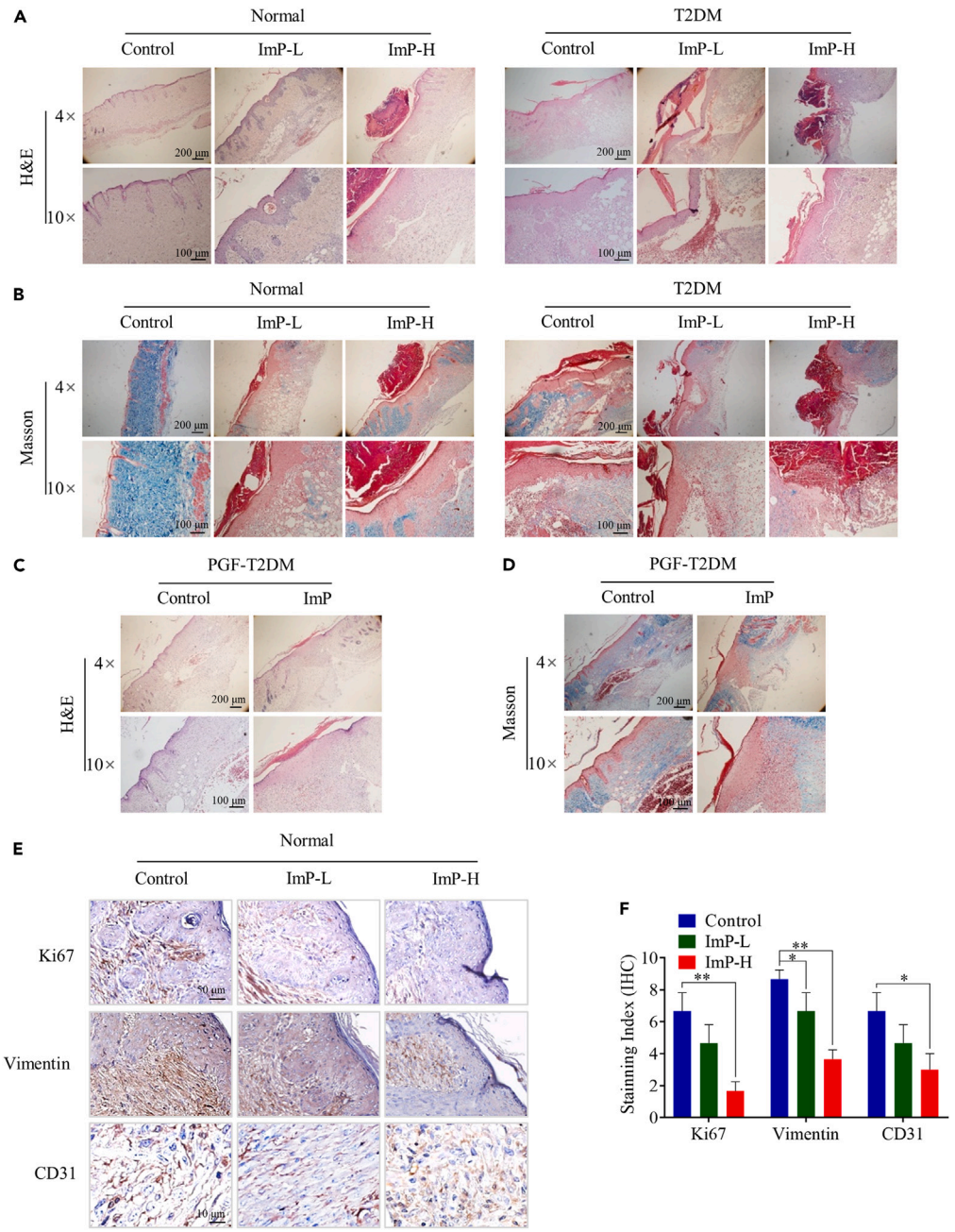

Figure 2. Effect of ImP on skin wound tissue morphology, collagen production, and wound healing-related protein markers

(A and B) H&E and Masson staining results of the skin tissue (obtained on day 9 after wounding) in the ImP-treated normal and T2DM groups. ImP-L: 700 nM, ImP-H: 1.5 μM, dermal topical administration.

(C and D) H&E and Masson staining results of the skin tissues (obtained on day 9 after wounding) in the PGF-T2DM group (ImP 2 mg/mL, intragastric administration).

(E) The effect of ImP on the expression of Ki67, vimentin, and CD31 in skin tissues detected by immunohistochemistry. ImP-L: 700 nM, ImP-H: 1.5 μM, dermal topical administration.

(F) The statistic results of Ki67, vimentin, and CD31 immunohistochemical scores. Data were expressed as mean ± SD (*$p < 0.05$, **$p < 0.01$). The number of sample replicates for all experiments was 6 ($n = 6$).

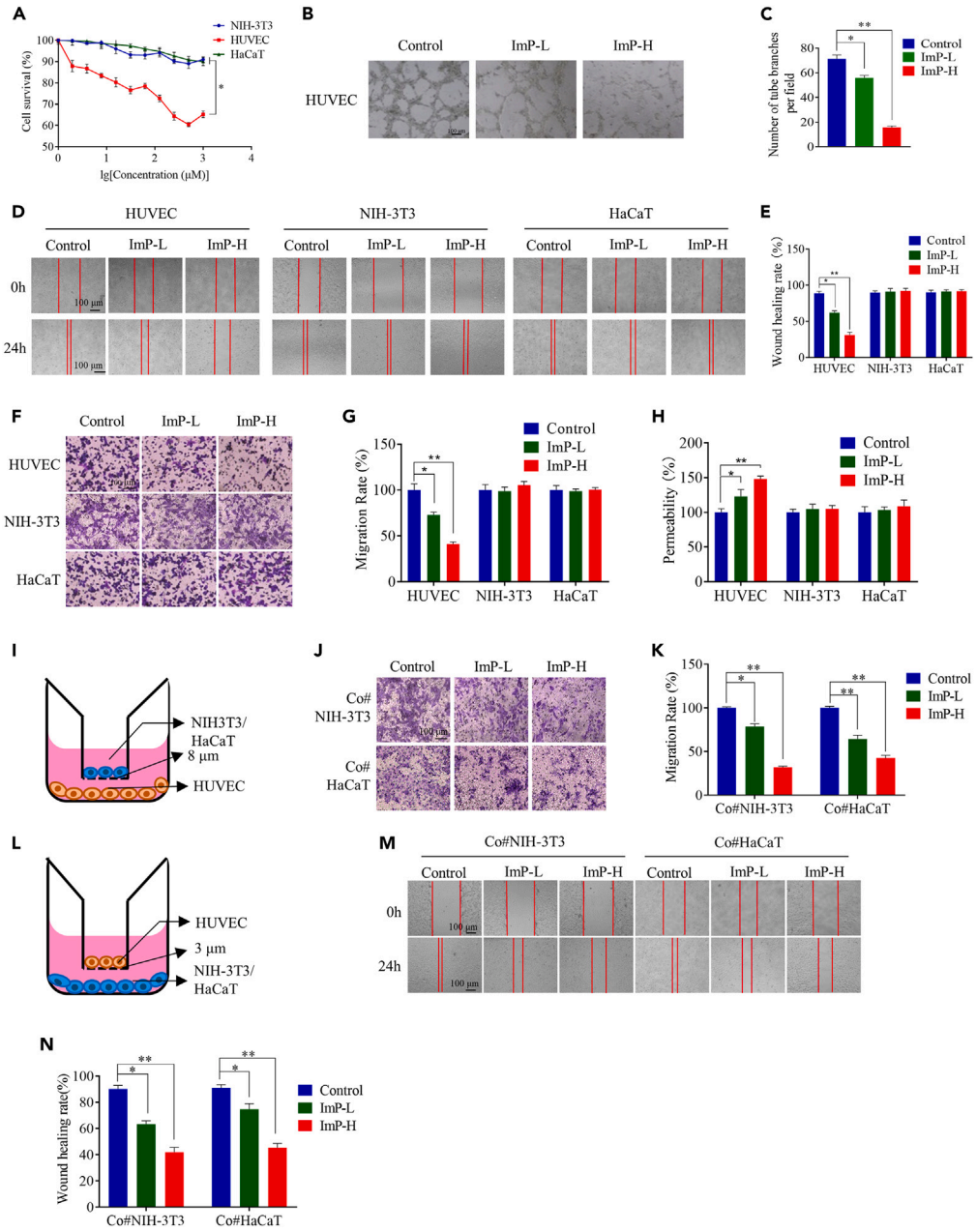

Figure 3. ImP inhibits the function of vascular endothelial cells without directly affecting the function of fibroblasts and epidermal cells

(A) The influence of ImP on the viability of HUVEC, NIH-3T3, and HaCaT cells.

(B and C) The effect of ImP on the angiogenesis ability of HUVEC cells.

(D and E) The impact of ImP on the migration ability of HUVEC, NIH-3T3, and HaCaT cells detected by scratch test.

(F and G) The effect of ImP on the migration ability of HUVEC, NIH-3T3, and HaCaT cells detected by transwell experiment.

(H) The effect of ImP on the permeability of HUVEC, NIH-3T3, and HaCaT cells.

(I) Schematic diagram of coculture model; the upper chamber was NIH-3T3 or HaCaT cells, and the lower chamber was HUVEC cells.

(J and K) The effect of ImP on the migration ability of NIH-3T3/HaCaT under cocultivation conditions (Co#NIH-3T3, Co#HaCaT).

(L) Schematic diagram of coculture model combined with scratch assay; the upper chamber was HUVEC cells, and the lower chamber was NIH-3T3 or HaCaT cells.

(M and N) The effect of ImP on wound healing in Co#NIH-3T3 or Co#HaCaT cells under coculture conditions. ImP-L: 500 nM, ImP-H: 1μM. Data are expressed as the mean ± SD (*$p < 0.05$, **$p < 0.01$). The number of sample replicates for all experiments was 6 ($n = 6$).

(Figures 3B and 3C). In this research, a scratch assay was used to detect the influence of ImP on the migration ability of the cells. The migration speed of HUVEC cells in the ImP-treated group was slower than that in the control group, indicating that ImP can inhibit the migration ability of HUVEC cells (Figures 3D and 3E). However, ImP exerted a slight effect on the migration ability of the NIH-3T3 and HaCaT cells. The results of the transwell experiment (Figures 3F and 3G) also showed that ImP can inhibit the migration ability of HUVEC cells in a dose-dependent manner. ImP had no significant effect on the migration ability of the NIH-3T3 and HaCaT cells. The endothelial cell permeability assay showed that the amount of TRITC–dextran passed through the HUVEC monolayer in the ImP-treated group was increased relative to that in the control group, indicating that ImP increased the cell permeability of HUVEC cells. ImP showed no obvious effect on the permeability of the NIH-3T3 and HaCaT cells. These results indicated that ImP mainly acted on vascular endothelial cells and had no direct effect on the functions of fibroblasts and epidermal cells.

To further study the mechanism by which ImP affects the migration of fibroblasts and keratinocytes in tissues, a coculture model of HUVEC and NIH-3T3/HaCaT (Co#NIH-3T3, Co#HaCaT) was established to simulate the interaction between vascular endothelial cells and fibroblasts or keratinocytes. NIH-3T3 or HaCaT cells were seeded to the upper part of the Transwell chamber, and HUVEC cells were seeded to the lower chamber (Figure 3I). ImP was added to the lower chamber at a dose of 500 nM and 1 μM. The pore size of the polycarbonate membrane on the bottom of the chamber was 8 μm to ensure that the upper chamber cells and soluble factors can pass through and ensure the material exchange between HUVEC and NIH-3T3/HaCaT. The migration ability of cells in the chamber was evaluated in different groups. The results showed that ImP can inhibit the migration of Co#NIH-3T3 and Co#HaCaT (Figures 3J and 3K). The effect of ImP on the migration ability of Co#NIH-3T3 and Co#HaCaT was further studied through the coculture model combined with the scratch experiment (Figures 3L–3N). Compared with the scratch test results of NIH-3T3 and HaCaT cultured separately, the migration ability of Co#NIH-3T3 and Co#HaCaT slowed down after the addition of ImP in a dose-dependent manner.

Imidazole propionate inhibited S1P release by targeting SPNS2 transport process

The above results showed that ImP mainly affects the angiogenesis and migration ability of HUVEC cells and the function of Co#NIH-3T3 (cocultured with HUVEC) and Co#HaCaT (cocultured with HUVEC). ImP had no obvious effects on NIH-3T3 and HaCaT cells cultured alone. The results indicated that ImP may affected the migration ability of fibroblasts and keratinocytes by inhibiting the release of cytokines after acting on vascular endothelial cells. S1P plays an important role in angiogenesis, cell migration and wound healing.[24,25] The main sources of S1P *in vivo* were hematopoietic and vascular endothelial cells. So we speculate ImP may affect S1P secretion in HUVEC cells, thereby affecting the migration ability of fibroblasts and keratinocytes. Therefore, the effect of ImP on S1P secretion was further tested. The intracellular and extracellular S1P levels of HUVEC cells were detected by ELISA experiments. The S1P content in the supernatant of HUVEC cell culture medium decreased compared with that in the control group, whereas intracellular S1P content increased (Figure 4A). Changes in S1P level in mice was detected. Figure 4B showed that the application of ImP to the skin wound decreased S1P content in the wound tissues and blood secretion. The S1P content in the wound tissues and blood secretion in T2DM mice were also significantly lower than those in the normal mice. After ImP was added, the S1P content further decreased. These results suggested that ImP disrupts the release of S1P.

SPNS2 is an important transporter of S1P in vascular endothelial cells.[26,27] Therefore, ImP may inhibit the SPNS2-mediated transport of S1P. To verify whether ImP affects SPNS2-mediated S1P transport, HUVEC cells transfected with SPNS2 siRNA (Si-SPNS2) were used. ImP had a weaker effect on the viability of Si-SPNS2 HUVEC cells than on the normal HUVEC cells (Figure 4C). ImP slightly affected angiogenesis (Figures 4D and 4E) and permeability (Figure 4F) in the Si-SPNS2 HUVEC cells. ImP also had no significant effect on the migration ability of Si-SPNS2 HUVEC and Co#NIH3T3cells cocultured with Si-SPNS2 HUVEC cells (Figures 4G and 4H). $SPNS2^{-/-}$ mice were used to establish a wound model to analyze whether ImP affects wound healing by regulating SPNS2-mediated S1P transport. Figures 4I and 4J show that the wound healing speed of $SPNS2^{-/-}$ mice was slower than that in the control group. And ImP posed no significant effect on the wound healing speed of $SPNS2^{-/-}$ mice. The number of CD31-positive cells in the skin wound tissues of the $SPNS2^{-/-}$ mice were fewer than those in the control mice. No significant difference in the number of CD31-positive cells in the skin wounds was found between $SPNS2^{-/-}$ mice and ImP-treated mice (Figures 4K and 4L). The results showed that ImP may inhibit wound healing by disrupting the release of S1P by targeting SPNS2 transport process (The CD31-positive cells in the skin tissue of the wound were determined to be evaluated by immunohistochemistry).

Imidazole propionate can inhibit S1P-induced Rho signaling pathway

Whether ImP can inhibit the downstream signaling pathway of S1P was evaluated through proteomics analysis. ImP- and S1P-treated HUVEC cells were analyzed by mass spectrometry. The down-regulated proteins in the ImP-treated group and the up-regulated proteins in the S1P-treated group were screened and analyzed by KEGG and GO analyses. Figures 5A and 5B showed that ImP can inhibit the multiple functions of vascular endothelial cells, such as cell migration, proliferation, and invasion. S1P up-regulated the cytoskeleton movement, proliferation, epithelial–mesenchymal transition, and other functions of the HUVEC cells. Pathway analysis showed that ImP mainly affected the Rho pathway. STRING analysis results were shown in Figure 5C. ImP affected vascular endothelial cell migration, proliferation, collagen production, cytoskeleton movement, and other related functions. We further evaluated the effect of ImP on wound healing related proteins.

Angiogenesis is an important process of wound healing,[28] and the formation of granulation tissues rich in blood vessels is a key step in tissue regeneration.[29,30] VEGF, CD31, and HIF-1α are the main markers associated with angiogenesis.[31–33] Therefore, Western blot was used to detect the effects of ImP on these proteins. The results showed that S1P can promote the expression of VEGF, CD31, and HIF-1α, whereas ImP inhibited their expression (Figures 5D and 5E). ImP inhibits the expression of cell proliferation marker Ki67,[34] and the expression of MMP-2 and MMP-9 at the edges of acute wounds is related to the migration of fibroblasts and keratinocyte.[35–37] Therefore,

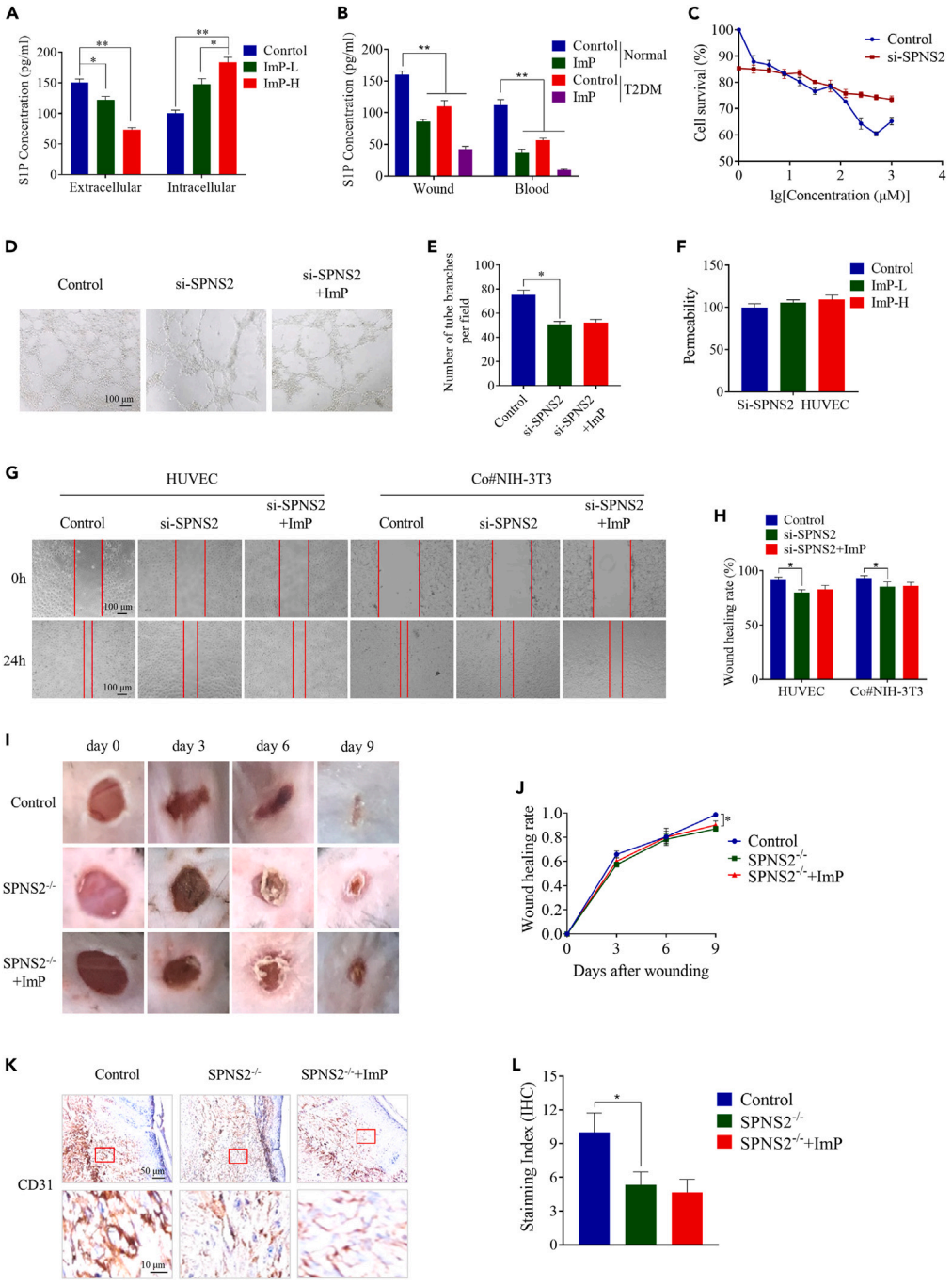

Figure 4. Effect of ImP on SPNS2-mediated S1P transport

(A) The impact of ImP on the S1P level in the extracellular and intracellular of HUVEC cells detected by ELISA (n = 3), ImP-L: 500 nM, ImP-H: 1μM.

(B) Changes in SIP level in wound tissues and blood secretion in normal and T2DM mice(n = 6), ImP: 1.5 μM.

(C) Effect of ImP on the viability of HUVEC cells and Si-SPNS2 HUVEC cells (n = 3), ImP:1 μM.

(D and E) The effect of ImP on the angiogenesis ability of Si-SPNS2 HUVEC cells (n = 3), ImP:1 μM.

(F) The effect of different doses of ImP on the permeability of Si-SPNS2 HUVEC cells.

(G and H) The effect of ImP on the migration of Si-SPNS2 HUVEC and NIH3T3cells under coculture conditions(n = 3), ImP:1 μM.

(I) The effect of ImP on skin wound healing in SPNS2$^{-/-}$ mice (n = 6), ImP:1.5 μM.

(J) Skin wound healing rate-time curves of ImP-treated SPNS2$^{-/-}$ mice.

(K and L) The effect of ImP on the expression of CD31 in the skin of SPNS2$^{-/-}$ mice detected by immunohistochemistry (n = 6), ImP:1.5 μM. Data were expressed as mean ± SD (*p < 0.05, **p < 0.01).

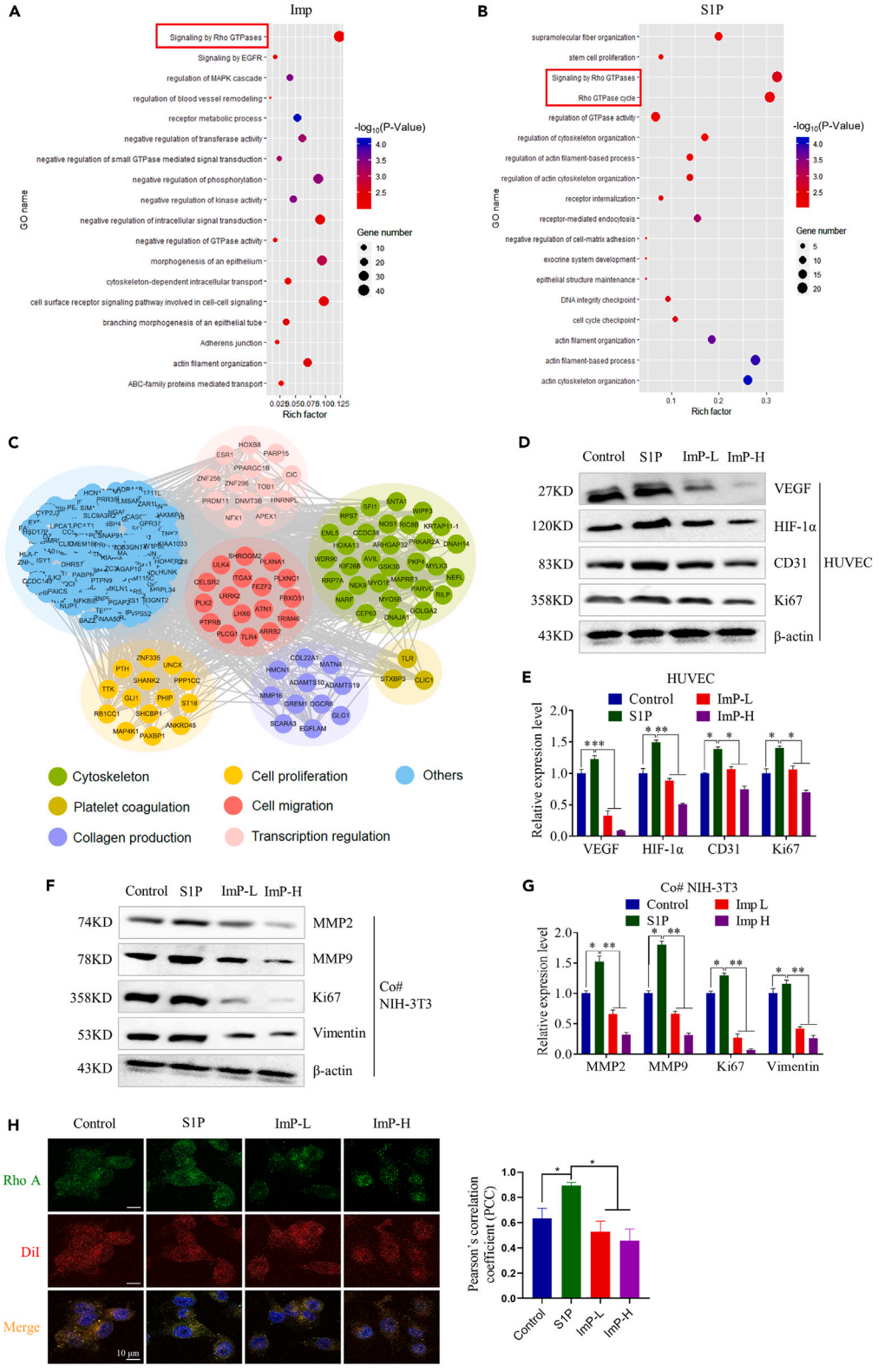

Figure 5. ImP played a role in regulating wound healing by inhibiting the downstream Rho pathway of S1P

(A and B) Functions and pathways negatively enriched for ImP treated cells and positively enriched for S1P treated cells were shown. The differentially expressed proteins was identified and analyzed by GO and KEGG pathway analysis.

Figure 5. *Continued*

(C) Protein-protein interaction network analysis of ImP down-regulating protein by STRING.

(D and E) The effects of S1P and ImP on the expression levels of VEGF, HIF-1α, CD31, and Ki67 proteins in HUVEC cells detected by Western blot.

(F and G) The effect of ImP and S1P on the protein expression levels of MMP2, MMP9, Ki67 and Vimentin in NIH3T3cells under coculture conditions.

(H) The effect of ImP on the cell membrane localization of RhoA. ImP-L:500 nM, ImP-H: 1μM. Data are expressed as the mean ± SD (*p < 0.05, **p < 0.01). The number of sample replicates for all experiments was 3 (n = 3).

the HUVEC/NIH-3T3 coculture model was also used to explore the effect of ImP on the related proteins in cocultured NIH-3T3 after the secretion of S1P in HUVEC cells was inhibited. ImP inhibited the expression of MMP2, MMP9, Ki67, and vimentin in the Co#NIH3T3cells, whereas S1P increased the expression of the proteins (Figures 5F and 5G). Proteomics analysis showed that ImP mainly affected the Rho pathway, which was an important pathway for S1P function.[38,39] The impact of ImP on the Rho pathway was evaluated by immunofluorescence. S1P promoted the transfer of Rho A on the cell membrane, which further activation the Rho pathway. ImP inhibited the localization of Rho A on the cell membrane. These results indicated that ImP can inhibit the activation of the Rho pathway (Figure 5H). Western blot images of the original blots were shown in Figure S3.

Small-molecule HMPA can promote skin wound healing in type 2 diabetes mellitus mice through gut microbiota regulation

As ImP is a metabolite of the gut microbiota associated with T2DM, the effect of the gut microbiota regulator HMPA, which we discovered in our previous research,[40] on wound healing in T2DM mice was evaluated. After the administration of HMPA, the genus abundance of gut microbiota changed compared with that in the normal group (Figure 6A). After the administration of HMPA, the abundance of *Prevotella* and *Ruminococcaceae* in the T2DM mice considerably changed. The abundance of *Streptococcus*, an ImP-producing bacterium, was significantly reduced in the HMPA-administered group. And the abundance of *Streptococcus* at the skin was also decreased in HMPA treated group (Figure 6B). The results of the T2DM skin wound healing model (Figures 6C and 6D) showed that HMPA promotes wound healing in T2DM mice. The expression of CD31 in the HMPA group increased relative to that in the T2DM group (Figures 6E and 6F). H&E and Masson staining results also showed that HMPA can promote the growth of skin tissues and collagen production (Figures 6G and 6H).

DISCUSSION

Delayed wound healing is a common phenomenon in patients with T2DM, seriously affects their quality of life, and is even life threatening.[41,42] Wound healing in these patients is slow, the infection rate was high, and the risk of lower limb amputation is significantly increased.[43–45] The gut microbiota, through its metabolites, can promote the progress of T2DM by regulating downstream metabolism, inflammation, immunity, and other signaling pathways.[46–48] It can directly or indirectly affect tissue oxygenation level, angiogenesis, inflammation, and immune system, thereby affecting wound healing.[49,50] The oral administration of some probiotics can reduce the size of foot ulcer wounds in patients with T2DM.[51] ImP is a metabolite of gut microbiota closely related to T2DM and can inhibit insulin signal transduction by activating the mTORC1 pathway.[13,52] It can also reduce the therapeutic effect of metformin on T2DM. Urocanate reductase (UrdA) can catalyze urocanate to produce ImP.[53] Karlsson et al. used metagenomics data to identify 42 bacterial strains with UrdA, of which 28 strains (67%) had a higher content in subjects with T2DM.[13] Among them, *Streptococcus mutans* and *Eggerthella lenta* (verified *in vitro* as an ImP-producing bacterium) were abundant in subjects with T2DM. The current study showed that the abundance of *Streptococcus mutans* in the intestine and skin of T2DM mice increased. In the *in vivo* experiment, a skin wound model was established to demonstrate that ImP can inhibit the skin wound healing in a dose-dependent manner. The T2DM animal model results showed that ImP delays the healing of T2DM wounds. These results showed that ImP, as a metabolite of gut microbiota, can inhibit wound healing process.

The inhibition of angiogenesis caused by vascular endothelial cell damage was one of the important reasons for the slow wound healing in patients with T2DM.[54] Vascular endothelial injury affects cell adhesion, vascular wall integrity, vascular permeability, blood flow regulation, and angiogenesis.[55,56] The characteristics of damaged endothelial cells included reduced angiogenesis, phenotypic changes, inflammation, and impaired permeability.[57,58] Local angiogenesis is reduced in patients with T2DM,[59] and decreased blood supply can lead to delayed wound healing. In addition, the reasons for the delayed wound healing of T2DM include the reduced migration and proliferation of keratinocytes and epidermal fibroblasts,[60,61] increased apoptosis, and reduced epithelial-to-mesenchymal transition (EMT).[62] In the present study, the effect of ImP on the function of vascular endothelial cells was evaluated. ImP inhibits the migration, proliferation, and angiogenesis of vascular endothelial cells, while posing little direct effect on the functions of fibroblasts and epidermal cells. By evaluating the expression of CD31 in wounded skin, we found that ImP can significantly inhibit the formation of blood vessels in wound tissues.

S1P is a sphingolipid metabolite with a wide range of biological activities and regulates cell growth, angiogenesis, lymphangiogenesis, and endothelial and epithelial barrier functions.[63,64] The S1P−S1PRs axis plays a key regulatory role in angiogenesis and vascular permeability, and S1P regulates angiogenesis by binding to S1PR1 and S1PR3 on vascular endothelial cells.[17] In addition, S1P can increase the adhesion and junction activity of endothelial cells. Owing to the high levels of S1P in the peripheral blood, S1P activity related to vascular permeability helps maintain the integrity of specific vascular endothelial barriers. S1P also regulates the migration of fibroblasts and epidermal cells and plays an important regulatory role in wound healing. The results of this study showed that ImP can affect the secretion (transport) of S1P in HUVEC cells. ImP can inhibit the migration of fibroblasts and epidermal cells cocultured with vascular endothelial cells and can affect the functions of fibroblasts and epidermal cells in the coculture environment by inhibiting the S1P secretion of HUVEC cells. SPNS2 is an important physiologically relevant transporter of S1P[65] in endothelial cells. This study verified that ImP can target SPNS2 to inhibit S1P transport through

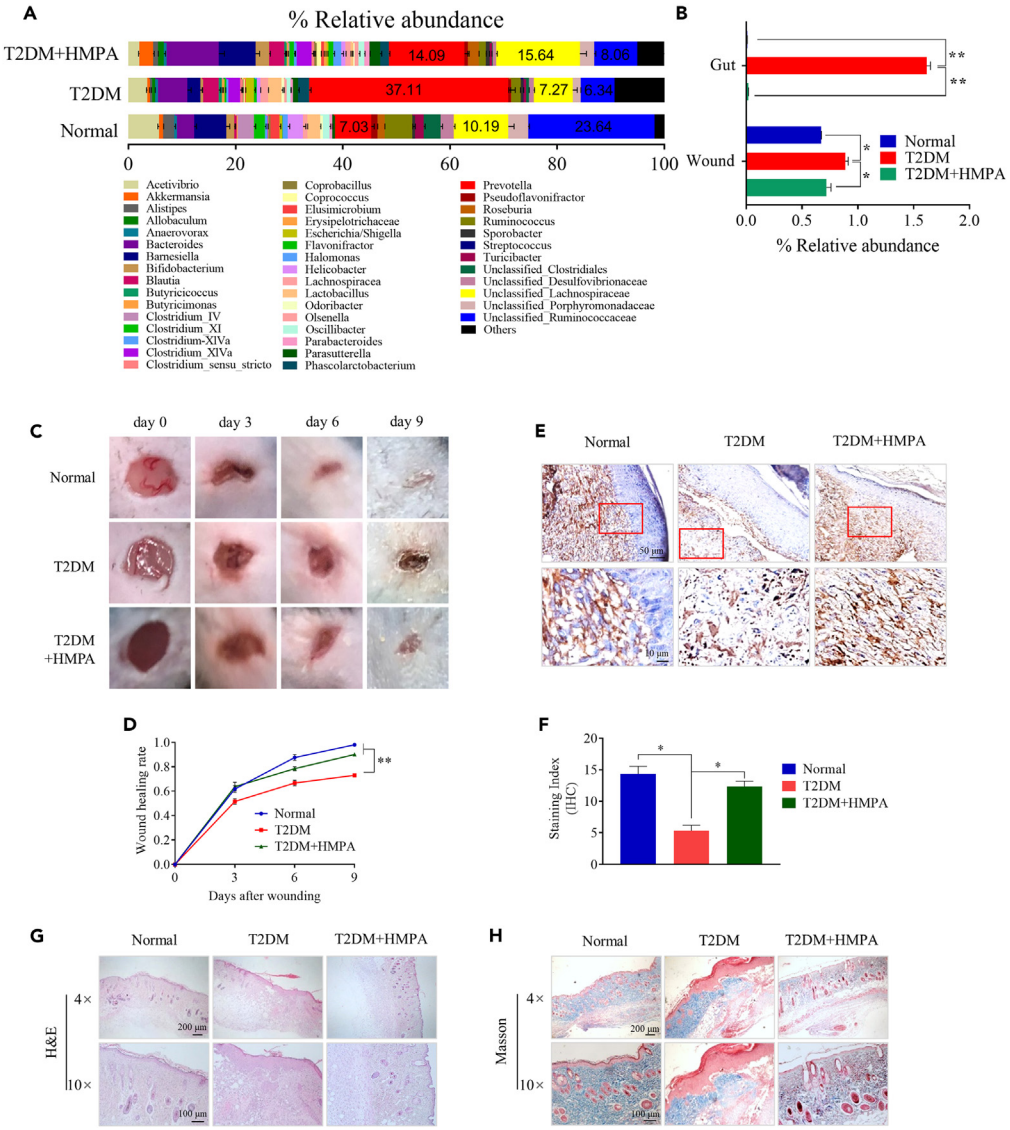

Figure 6. Effect of HMPA on skin wound healing in T2DM mice

(A) Difference in gut microbiota abundance at the genus level in T2DM mice after the administration of HMPA.

(B) The difference in the abundance of *Streptococcus* in the intestines and skin of the T2DM group after HMPA administration.

(C) The effect of HMPA administration on wound healing in the skin of T2DM mice.

(D) Skin wound healing rate-time curves of T2DM mice after the administration of HMPA.

(E and F) The effect of HMPA administration on the expression of CD31 in the skin wound tissue detected by immunohistochemistry.

(G and H) H&E and Masson staining results of skin wound tissues 9 days after HMPA administration. HMPA: 15 mg/kg, intragastric administration. Data were expressed as mean ± SD (*$p < 0.05$, **$p < 0.01$). The number of sample replicates for all experiments was 6 ($n = 6$).

the Si-SPNS2 HUVEC cells and SPNS2$^{-/-}$ mice experiment. The Rho signaling pathway is an important pathway for S1P to regulate angiogenesis. S1P can induce the reorganization of the actin cytoskeleton by activating GTPase Rho and contribute to the chemotactic and angiogenic activity of HUVEC cells.[66] In the present study, ImP inhibited the activation of the Rho signaling pathway, and decreased the expression of angiogenic related proteins VEGF, CD31, HIF-1α, and Ki67 in HUVEC cells. The expression levels of MMP2, MMP9, Ki67, and vimentin related to cell migration and movement in cocultured NIH3T3cells decreased, indicating that ImP plays an important role in wound healing at the molecular level. The effect of the small-molecule drug HMPA on wound healing was also evaluated. HMPA regulated the abundance of the ImP-producing bacterium *Streptococcus* and accelerated wound healing in T2DM wound mice. This study only provides a preliminary explanation of the effects of ImP on skin wound healing and its impact on the S1P pathway at the cellular and experimental animal levels. Due to the complexity of gut microbiota and its metabolites, the impact of ImP on wound healing in patients with T2DM may be more

complex, and further research evidence is needed. And the effect of HMPA on T2DM wound healing also needs further verification and improvement.

In conclusion, we found that the ImP-producing bacterium Stre*ptococcus* has a high abundance in the skin wounds of the T2DM mice. ImP inhibits the SPNS2 mediated transport of S1P, induces the injury of vascular endothelial cells, and inhibits T2DM wound healing. The intestinal microbiota regulator HMPA reduced the abundance of ImP-producing *Streptococcus* and promoted wound healing in T2DM mice. This study provides a basis for clarifying the relationship between gut microbiota and T2DM wound healing and provides a potential drug for promoting wound healing.

Limitations of the study

This study focused on the effects of ImP on vascular endothelial injury and T2DM wound healing, and found that ImP inhibited SPNS2-induced S1P transport process. However, how ImP inhibits SPNS2-mediated S1P transport needs to be further studied.

STAR★METHODS

Detailed methods are provided in the online version of this paper and include the following:

- KEY RESOURCES TABLE
- RESOURCE AVAILABILITY
  - Lead contact
  - Materials availability
  - Data and code availability
- EXPERIMENTAL MODEL AND STUDY PARTICIPANT DETAILS
  - Cell culture
  - Animal
- METHOD DETAILS
  - Cell transfection
  - Western blot
  - Cell viability experiment
  - Transwell migration assay
  - Internal cell permeability test
  - Wound healing assay
  - Immunofluorescence
  - qPCR
  - Proteomics analysis
  - Animal experiments
  - 16 S rRNA sequencing and functional analysis
  - Immunohistochemistry
- QUANTIFICATION AND STATISTICAL ANALYSIS

SUPPLEMENTAL INFORMATION

Supplemental information can be found online at https://doi.org/10.1016/j.isci.2023.108092.

ACKNOWLEDGMENTS

This work was supported by the National Natural Science Foundation of China (grant nos. 82273237, 82272934, and 82073205), the China Postdoctoral Science Foundation (nos. 2021M701778, 2022M721720), the National Youth Talent Support Program (2020), the Tianjin Science Fund for Distinguished Young Scholars (19JCJQJC63200), the Tianjin Natural Science Foundation (21JCZDJC00930), the Fundamental Research Funds for the Central Universities (Nankai University), (grant no. 735-63233164) and Hundred Young Academic Leaders Program of Nankai University.

The authors thank the instrument platform of the State Key Laboratory of Medicinal Chemical Biology and the Animal Laboratory Center of Tianjin Biomedical International Joint Research Institute for their assistance in cell and animal experiments. We are very grateful to the Home for Researchers website for its support in scientific mapping.

AUTHOR CONTRIBUTIONS

HJL and TS conceived and designed the experiment. All experiments were carried out by STZ and HQW. HQW, JXH, XTD, and YL analyzed the data. HJL and STZ wrote the article. All authors read and approved the final article.

DECLARATION OF INTERESTS

All authors have declared that they have no conflict of interest.

INCLUSION AND DIVERSITY

We support inclusive, diverse, and equitable conduct of research.

Received: February 7, 2023
Revised: July 20, 2023
Accepted: September 26, 2023
Published: September 28, 2023

REFERENCES

1. Zimmet, P., Alberti, K.G., and Shaw, J. (2001). Global and societal implications of the diabetes epidemic. Nature *414*, 782–787. https://doi.org/10.1038/414782a.
2. Saeedi, P., Petersohn, I., Salpea, P., Malanda, B., Karuranga, S., Unwin, N., Colagiuri, S., Guariguata, L., Motala, A.A., Ogurtsova, K., et al. (2019). Global and regional diabetes prevalence estimates for 2019 and projections for 2030 and 2045: Results from the International Diabetes Federation Diabetes Atlas, 9(th) edition. Diabetes Res. Clin. Pract. *157*, 107843. https://doi.org/10.1016/j.diabres.2019.107843.
3. Falanga, V. (2005). Wound healing and its impairment in the diabetic foot. Lancet *366*, 1736–1743. https://doi.org/10.1016/s0140-6736(05)67700-8.
4. Wu, X., Alberico, S., Saidu, E., Rahman Khan, S., Zheng, S., Romero, R., Sik Chae, H., Li, S., Mochizuki, A., and Anders, J. (2015). Organic light emitting diode improves diabetic cutaneous wound healing in rats. Wound Repair Regen. *23*, 104–114. https://doi.org/10.1111/wrr.12258.
5. Okonkwo, U.A., and DiPietro, L.A. (2017). Diabetes and Wound Angiogenesis. Int. J. Mol. Sci. *18*, 1419. https://doi.org/10.3390/ijms18071419.
6. Singh, N., Armstrong, D.G., and Lipsky, B.A. (2005). Preventing foot ulcers in patients with diabetes. JAMA *293*, 217–228. https://doi.org/10.1001/jama.293.2.217.
7. Dumville, J.C., Lipsky, B.A., Hoey, C., Cruciani, M., Fiscon, M., and Xia, J. (2017). Topical antimicrobial agents for treating foot ulcers in people with diabetes. Cochrane Database Syst. Rev. *6*, Cd011038. https://doi.org/10.1002/14651858.CD011038.pub2.
8. Han, X., Wu, P., Li, L., Sahal, H.M., Ji, C., Zhang, J., Wang, Y., Wang, Q., Qian, H., Shi, H., and Xu, W. (2021). Exosomes derived from autologous dermal fibroblasts promote diabetic cutaneous wound healing through the Akt/β-catenin pathway. Cell Cycle *20*, 616–629. https://doi.org/10.1080/15384101.2021.1894813.
9. Qin, J., Li, Y., Cai, Z., Li, S., Zhu, J., Zhang, F., Liang, S., Zhang, W., Guan, Y., Shen, D., et al. (2012). A metagenome-wide association study of gut microbiota in type 2 diabetes. Nature *490*, 55–60. https://doi.org/10.1038/nature11450.
10. Koh, A., De Vadder, F., Kovatcheva-Datchary, P., and Bäckhed, F. (2016). From Dietary Fiber to Host Physiology: Short-Chain Fatty Acids as Key Bacterial Metabolites. Cell *165*, 1332–1345. https://doi.org/10.1016/j.cell.2016.05.041.
11. Adeva, M.M., Calviño, J., Souto, G., and Donapetry, C. (2012). Insulin resistance and the metabolism of branched-chain amino acids in humans. Amino Acids *43*, 171–181. https://doi.org/10.1007/s00726-011-1088-7.
12. Bloomgarden, Z. (2018). Diabetes and branched-chain amino acids: What is the link? J. Diabetes *10*, 350–352. https://doi.org/10.1111/1753-0407.12645.
13. Koh, A., Molinaro, A., Ståhlman, M., Khan, M.T., Schmidt, C., Mannerås-Holm, L., Wu, H., Carreras, A., Jeong, H., Olofsson, L.E., et al. (2018). Microbially Produced Imidazole Propionate Impairs Insulin Signaling through mTORC1. Cell *175*, 947–961.e17. https://doi.org/10.1016/j.cell.2018.09.055.
14. Edmonds, Y., Milstien, S., and Spiegel, S. (2011). Development of small-molecule inhibitors of sphingosine-1-phosphate signaling. Pharmacol. Ther. *132*, 352–360. https://doi.org/10.1016/j.pharmthera.2011.08.004.
15. Rosen, H., Stevens, R.C., Hanson, M., Roberts, E., and Oldstone, M.B.A. (2013). Sphingosine-1-phosphate and its receptors: structure, signaling, and influence. Annu. Rev. Biochem. *82*, 637–662. https://doi.org/10.1146/annurev-biochem-062411-130916.
16. Spiegel, S., and Milstien, S. (2011). The outs and the ins of sphingosine-1-phosphate in immunity. Nat. Rev. Immunol. *11*, 403–415. https://doi.org/10.1038/nri2974.
17. Lee, M.J., Thangada, S., Claffey, K.P., Ancellin, N., Liu, C.H., Kluk, M., Volpi, M., Sha'afi, R.I., and Hla, T. (1999). Vascular endothelial cell adherens junction assembly and morphogenesis induced by sphingosine-1-phosphate. Cell *99*, 301–312. https://doi.org/10.1016/s0092-8674(00)81661-x.
18. Wang, Z., Zheng, Y., Wang, F., Zhong, J., Zhao, T., Xie, Q., Zhu, T., Ma, F., Tang, Q., Zhou, B., and Zhu, J. (2020). Mfsd2a and Spns2 are essential for sphingosine-1-phosphate transport in the formation and maintenance of the blood-brain barrier. Sci. Adv. *6*, eaay8627. https://doi.org/10.1126/sciadv.aay8627.
19. Mendoza, A., Fang, V., Chen, C., Serasinghe, M., Verma, A., Muller, J., Chaluvadi, V.S., Dustin, M.L., Hla, T., Elemento, O., et al. (2017). Lymphatic endothelial S1P promotes mitochondrial function and survival in naive T cells. Nature *546*, 158–161. https://doi.org/10.1038/nature22352.
20. Miller, I., Min, M., Yang, C., Tian, C., Gookin, S., Carter, D., and Spencer, S.L. (2018). Ki67 is a Graded Rather than a Binary Marker of Proliferation versus Quiescence. Cell Rep. *24*, 1105–1112.e5. https://doi.org/10.1016/j.celrep.2018.06.110.
21. Talbott, H.E., Mascharak, S., Griffin, M., Wan, D.C., and Longaker, M.T. (2022). Wound healing, fibroblast heterogeneity, and fibrosis. Cell Stem Cell *29*, 1161–1180. https://doi.org/10.1016/j.stem.2022.07.006.
22. Werner, S., Krieg, T., and Smola, H. (2007). Keratinocyte-fibroblast interactions in wound healing. J. Invest. Dermatol. *127*, 998–1008. https://doi.org/10.1038/sj.jid.5700786.
23. Yang, M., Li, C.J., Sun, X., Guo, Q., Xiao, Y., Su, T., Tu, M.L., Peng, H., Lu, Q., Liu, Q., et al. (2017). MiR-497 approximately 195 cluster regulates angiogenesis during coupling with osteogenesis by maintaining endothelial Notch and HIF-1alpha activity. Nat. Commun. *8*, 16003. https://doi.org/10.1038/ncomms16003.
24. Cartier, A., and Hla, T. (2019). Sphingosine 1-phosphate: Lipid signaling in pathology and therapy. Science *366*, eaar5551. https://doi.org/10.1126/science.aar5551.
25. Zhang, J., Dunk, C.E., and Lye, S.J. (2013). Sphingosine signalling regulates decidual NK cell angiogenic phenotype and trophoblast migration. Hum. Reprod. *28*, 3026–3037. https://doi.org/10.1093/humrep/det339.
26. Laurenzana, A., Cencetti, F., Serratì, S., Bruno, G., Japtok, L., Bianchini, F., Torre, E., Fibbi, G., Del Rosso, M., Bruni, P., and Donati, C. (2015). Endothelial sphingosine kinase/SPNS2 axis is critical for vessel-like formation by human mesoangioblasts. J. Mol. Med. *93*, 1145–1157. https://doi.org/10.1007/s00109-015-1292-0.
27. Fu, P., Ebenezer, D.L., Berdyshev, E.V., Bronova, I.A., Shaaya, M., Harijith, A., and Natarajan, V. (2016). Role of Sphingosine Kinase 1 and S1P Transporter Spns2 in HGF-mediated Lamellipodia Formation in Lung Endothelium. J. Biol. Chem. *291*, 27187–27203. https://doi.org/10.1074/jbc.M116.758946.
28. DiPietro, L.A. (2016). Angiogenesis and wound repair: when enough is enough. J. Leukoc. Biol. *100*, 979–984. https://doi.org/10.1189/jlb.4MR0316-102R.
29. Desmoulière, A., Badid, C., Bochaton-Piallat, M.L., and Gabbiani, G. (1997). Apoptosis during wound healing, fibrocontractive diseases and vascular wall injury. Int. J. Biochem. Cell Biol. *29*, 19–30. https://doi.org/10.1016/s1357-2725(96)00117-3.
30. Eming, S.A., Wynn, T.A., and Martin, P. (2017). Inflammation and metabolism in tissue repair and regeneration. Science *356*, 1026–1030. https://doi.org/10.1126/science.aam7928.
31. Apte, R.S., Chen, D.S., and Ferrara, N. (2019). VEGF in Signaling and Disease: Beyond Discovery and Development. Cell *176*, 1248–

1264. https://doi.org/10.1016/j.cell.2019.01.021.
32. Peng, Y., Wu, S., Li, Y., and Crane, J.L. (2020). Type H blood vessels in bone modeling and remodeling. Theranostics *10*, 426–436. https://doi.org/10.7150/thno.34126.
33. Chen, Y., Fu, L., Han, Y., Teng, Y., Sun, J., Xie, R., and Cao, J. (2012). Testosterone replacement therapy promotes angiogenesis after acute myocardial infarction by enhancing expression of cytokines HIF-1a, SDF-1a and VEGF. Eur. J. Pharmacol. *684*, 116–124. https://doi.org/10.1016/j.ejphar.2012.03.032.
34. Menon, S.S., Guruvayoorappan, C., Sakthivel, K.M., and Rasmi, R.R. (2019). Ki-67 protein as a tumour proliferation marker. Clin. Chim. Acta *491*, 39–45. https://doi.org/10.1016/j.cca.2019.01.011.
35. Moses, M.A., Marikovsky, M., Harper, J.W., Vogt, P., Eriksson, E., Klagsbrun, M., and Langer, R. (1996). Temporal study of the activity of matrix metalloproteinases and their endogenous inhibitors during wound healing. J. Cell. Biochem. *60*, 379–386. https://doi.org/10.1002/(sici)1097-4644(19960301)60:3%3c379::Aid-jcb9%3e3.0.Co;2-t.
36. Wells, J.M., Gaggar, A., and Blalock, J.E. (2015). MMP generated matrikines. Matrix Biol. *44–46*, 122–129. https://doi.org/10.1016/j.matbio.2015.01.016.
37. Martins, V.L., Caley, M., and O'Toole, E.A. (2013). Matrix metalloproteinases and epidermal wound repair. Cell Tissue Res. *351*, 255–268. https://doi.org/10.1007/s00441-012-1410-z.
38. Zhang, R., Feng, X., Zhan, M., Huang, C., Chen, K., Tang, X., Kang, T., Xiong, Y., and Lei, M. (2016). Transcription Factor Sp1 Promotes the Expression of Porcine ROCK1 Gene. Int. J. Mol. Sci. *17*, 112. https://doi.org/10.3390/ijms17010112.
39. Gudipaty, S.A., and Rosenblatt, J. (2017). Epithelial cell extrusion: Pathways and pathologies. Semin. Cell Dev. Biol. *67*, 132–140. https://doi.org/10.1016/j.semcdb.2016.05.010.
40. Liu, H., Qin, Y., Li, K., Li, M., Yang, J., Tao, H., Tang, Y., Yang, L., Chen, S., Liu, Y., et al. (2021). Potential type 2 diabetes mellitus drug HMPA promotes short-chain fatty acid production by improving carbon catabolite repression effect of gut microbiota. Br. J. Pharmacol. *178*, 946–963. https://doi.org/10.1111/bph.15338.
41. Xiong, Y., Chen, L., Yan, C., Zhou, W., Endo, Y., Liu, J., Hu, L., Hu, Y., Mi, B., and Liu, G. (2020). Circulating Exosomal miR-20b-5p Inhibition Restores Wnt9b Signaling and Reverses Diabetes-Associated Impaired Wound Healing. Small *16*, e1904044. https://doi.org/10.1002/smll.201904044.
42. Wong, Y.H., Wong, S.H., Wong, X.T., Yap, Q.Y., Yip, K.Y., Wong, L.Z., Chellappan, D.K., Bhattamisra, S.K., and Candasamy, M. (2022). Genetic associated complications of type 2 diabetes mellitus. Panminerva Med. *64*, 274–288. https://doi.org/10.23736/S0031-0808.21.04285-3.
43. Kar, A.K., Singh, A., Singh, D., Shraogi, N., Verma, R., Saji, J., Jagdale, P., Ghosh, D., and Patnaik, S. (2022). Biopolymeric composite hydrogel loaded with silver NPs and epigallocatechin gallate (EGCG) effectively manages ROS for rapid wound healing in type II diabetic wounds. Int. J. Biol. Macromol. *218*, 506–518. https://doi.org/10.1016/j.ijbiomac.2022.06.196.
44. Chen, Z., Haus, J.M., DiPietro, L.A., Koh, T.J., and Minshall, R.D. (2023). Neutralization of excessive CCL28 improves wound healing in diabetic mice. Front. Pharmacol. *14*, 1087924. https://doi.org/10.3389/fphar.2023.1087924.
45. Littig, J.P.B., Moellmer, R., Agrawal, D.K., and Rai, V. (2023). Future applications of exosomes delivering resolvins and cytokines in facilitating diabetic foot ulcer healing. World J. Diabetes *14*, 35–47. https://doi.org/10.4239/wjd.v14.i1.35.
46. Ma, Q., Li, Y., Li, P., Wang, M., Wang, J., Tang, Z., Wang, T., Luo, L., Wang, C., Wang, T., and Zhao, B. (2019). Research progress in the relationship between type 2 diabetes mellitus and intestinal flora. Biomed. Pharmacother. *117*, 109138. https://doi.org/10.1016/j.biopha.2019.109138.
47. Liu, L., Zhang, J., Cheng, Y., Zhu, M., Xiao, Z., Ruan, G., and Wei, Y. (2022). Gut microbiota: A new target for T2DM prevention and treatment. Front. Endocrinol. *13*, 958218. https://doi.org/10.3389/fendo.2022.958218.
48. Tanase, D.M., Gosav, E.M., Neculae, E., Costea, C.F., Ciocoiu, M., Hurjui, L.L., Tarniceriu, C.C., Maranduca, M.A., Lacatusu, C.M., Floria, M., and Serban, I.L. (2020). Role of Gut Microbiota on Onset and Progression of Microvascular Complications of Type 2 Diabetes (T2DM). Nutrients *12*, 3719. https://doi.org/10.3390/nu12123719.
49. Patel, B.K., Patel, K.H., Huang, R.Y., Lee, C.N., and Moochhala, S.M. (2022). The Gut-Skin Microbiota Axis and Its Role in Diabetic Wound Healing-A Review Based on Current Literature. Int. J. Mol. Sci. *23*, 2375. https://doi.org/10.3390/ijms23042375.
50. Wang, Y., Zhang, H., Ma, G., Tian, Z., and Wang, B. (2022). The contribution of intestinal Streptococcus to the pathogenesis of diabetic foot ulcers: An analysis based on 16S rRNA sequencing. Int. Wound J. *19*, 1658–1668. https://doi.org/10.1111/iwj.13766.
51. Mohseni, S., Bayani, M., Bahmani, F., Tajabadi-Ebrahimi, M., Bayani, M.A., Jafari, P., and Asemi, Z. (2018). The beneficial effects of probiotic administration on wound healing and metabolic status in patients with diabetic foot ulcer: A randomized, double-blind, placebo-controlled trial. Diabetes. Metab. Res. Rev. *34*. https://doi.org/10.1002/dmrr.2970.
52. Fang, X., Miao, R., Wei, J., Wu, H., and Tian, J. (2022). Advances in multi-omics study of biomarkers of glycolipid metabolism disorder. Comput. Struct. Biotechnol. J. *20*, 5935–5951. https://doi.org/10.1016/j.csbj.2022.10.030.
53. Venskutonytė, R., Koh, A., Stenström, O., Khan, M.T., Lundqvist, A., Akke, M., Bäckhed, F., and Lindkvist-Petersson, K. (2021). Structural characterization of the microbial enzyme urocanate reductase mediating imidazole propionate production. Nat. Commun. *12*, 1347. https://doi.org/10.1038/s41467-021-21548-y.
54. Morel, O., Jesel, L., Abbas, M., and Morel, N. (2013). Prothrombotic changes in diabetes mellitus. Semin. Thromb. Hemost. *39*, 477–488. https://doi.org/10.1055/s-0033-1343888.
55. Murakami, M., and Simons, M. (2009). Regulation of vascular integrity. J. Mol. Med. *87*, 571–582. https://doi.org/10.1007/s00109-009-0463-2.
56. Kaur, R., Kaur, M., and Singh, J. (2018). Endothelial dysfunction and platelet hyperactivity in type 2 diabetes mellitus: molecular insights and therapeutic strategies. Cardiovasc. Diabetol. *17*, 121. https://doi.org/10.1186/s12933-018-0763-3.
57. Gimbrone, M.A., Jr., and García-Cardeña, G. (2016). Endothelial Cell Dysfunction and the Pathobiology of Atherosclerosis. Circ. Res. *118*, 620–636. https://doi.org/10.1161/circresaha.115.306301.
58. Meza, C.A., La Favor, J.D., Kim, D.H., and Hickner, R.C. (2019). Endothelial Dysfunction: Is There a Hyperglycemia-Induced Imbalance of NOX and NOS? Int. J. Mol. Sci. *20*, 3775. https://doi.org/10.3390/ijms20153775.
59. Ackermann, M., Pabst, A.M., Houdek, J.P., Ziebart, T., and Konerding, M.A. (2014). Priming with proangiogenic growth factors and endothelial progenitor cells improves revascularization in linear diabetic wounds. Int. J. Mol. Med. *33*, 833–839. https://doi.org/10.3892/ijmm.2014.1630.
60. Wall, I.B., Moseley, R., Baird, D.M., Kipling, D., Giles, P., Laffafian, I., Price, P.E., Thomas, D.W., and Stephens, P. (2008). Fibroblast dysfunction is a key factor in the non-healing of chronic venous leg ulcers. J. Invest. Dermatol. *128*, 2526–2540. https://doi.org/10.1038/jid.2008.114.
61. Wilkinson, H.N., and Hardman, M.J. (2020). Wound healing: cellular mechanisms and pathological outcomes. Open Biol. *10*, 200223. https://doi.org/10.1098/rsob.200223.
62. Stone, R.C., Pastar, I., Ojeh, N., Chen, V., Liu, S., Garzon, K.I., and Tomic-Canic, M. (2016). Epithelial-mesenchymal transition in tissue repair and fibrosis. Cell Tissue Res. *365*, 495–506. https://doi.org/10.1007/s00441-016-2464-0.
63. Herzinger, T., Kleuser, B., Schäfer-Korting, M., and Korting, H.C. (2007). Sphingosine-1-phosphate signaling and the skin. Am. J. Clin. Dermatol. *8*, 329–336. https://doi.org/10.2165/00128071-200708060-00002.
64. Huang, W.C., Nagahashi, M., Terracina, K.P., and Takabe, K. (2013). Emerging Role of Sphingosine-1-phosphate in Inflammation, Cancer, and Lymphangiogenesis. Biomolecules *3*, 408–434. https://doi.org/10.3390/biom3030408.
65. Tanaka, S., Zheng, S., Kharel, Y., Fritzemeier, R.G., Huang, T., Foster, D., Poudel, N., Goggins, E., Yamaoka, Y., Rudnicka, K.P., et al. (2022). Sphingosine 1-phosphate signaling in perivascular cells enhances inflammation and fibrosis in the kidney. Sci. Transl. Med. *14*, eabj2681. https://doi.org/10.1126/scitranslmed.abj2681.
66. Gratzinger, D., Canosa, S., Engelhardt, B., and Madri, J.A. (2003). Platelet endothelial cell adhesion molecule-1 modulates endothelial cell motility through the small G-protein Rho. Faseb. J. *17*, 1458–1469. https://doi.org/10.1096/fj.02-1040com.

STAR★METHODS

KEY RESOURCES TABLE

REAGENT or RESOURCE	SOURCE	IDENTIFIER
Antibodies		
CD31	Affnity	Affinity Biosciences Cat# AF6191, RRID:AB_2835074.
VEGF	Affnity	Affinity Biosciences Cat# AF5131, RRID:AB_2837617.
HIF-1α	Affnity	Affinity Biosciences Cat# AF1009, RRID:AB_2835328.
Vimentin	Affinity	Affinity Biosciences Cat# AF7013, RRID:AB_2835318.
MMP2	Affinity	Affinity Biosciences Cat# AF5330, RRID:AB_2837815.
MMP9	Affinity	Affinity Biosciences Cat# AF5228, RRID:AB_2837714.
Ki67	Affinity	Affinity Biosciences Cat# AF0198, RRID:AB_2834152.
β-actin	Affinity	Affinity Biosciences Cat# AF7018, RRID:AB_2839420.
Chemicals, peptides, and recombinant proteins		
DMSO	Sigma	Cat# 67-68-5
Si-SPNS2 siRNA	Qingke Biotechnology Co., Ltd, Beijing, China	N/A
DMEM	Gibco	11965092
RIPA Lysis Buffer (medium)	Shanghai yuanye Bio-Technology Co., Ltd	R21236
Phosphate buffered solution	Solarbio	P1010
Matrigel matrix glue	Corning	356234
Masson's Trichrome Stain Kit	Solarbio	G1340
BCA Kit	Beyotime	P0011
S1P ELISA Kit	MEIMIAN Bio-Technology Co., Ltd	MM-13079H2
Experimental models: Cell lines		
HUVEC	KeyGen Biotech (Nanjing, China)	N/A
NIH-3T3	KeyGen Biotech (Nanjing, China)	N/A
HaCaT	KeyGen Biotech (Nanjing, China)	N/A
Experimental models: Animal		
Mouse：BALB/c	vitalriver	N/A
Software and algorithms		
ImageJ	Schneider et al.	https://imagej.net/
GraphPad Prism (version 7)	GraphPad Software	www.graphpad.com

RESOURCE AVAILABILITY

Lead contact

Further information and requests for resources should be directed to and will be fulfilled by the lead contact, Huijuan Liu (liuhuijuanxyz@163.com).

Materials availability

This study did not generate new unique reagents.

Data and code availability

- All data reported in this paper will be shared by the lead contact upon request.
- This paper does not report any original code.
- Any additional information required to reanalyse the data reported in this work is available from the lead contact upon reasonable request.

EXPERIMENTAL MODEL AND STUDY PARTICIPANT DETAILS

Cell culture

Fibroblasts (NIH-3T3), vascular endothelial cells (HUVEC), and keratinocytes (HaCaT) were purchased from KeyGEN BioTECH. Mycoplasma was analyzed using a mycoplasma quantitative polymerase chain reaction detection kit. The cells were grown in Dulbecco's modified Eagle's medium (DMEM) supplemented with 10% FBS and maintained at 37°C in a humidified atmosphere containing 5% CO_2.

Animal

T2DM animal models and skin wound models were established with wild-type BALB/c male mice (6 weeks old). All mice were kept in animal care facilities and were free of specific pathogens. All animal studies were conducted in accordance with the National Institutes of Health's animal use guidelines and the current Chinese laboratory animal use regulations and standards. All animal experiments were approved by the animal ethics committee of Tianjin International Joint Research Institute of Biomedicine and were carried out in accordance with experimental specifications.

METHOD DETAILS

Cell transfection

Si-SPNS2 siRNA was used for cell transfection experiments. Approximately 1.5 μg of Si-SPNS2 and 7.5 μL of Lipofectamine 2000 transfection reagent were added to 100 μL of Opti-MEM successively, which was incubated at room temperature for 15 min. At 60% cell density and good growth, the siRNA mixture was added to the cells and cultured in 2% serum for 8 h, the medium was then changed to full medium and incubation was continued for 24-48h.

Western blot

The collected cells were washed with cold PBS and lysed in RIPA lysis buffer for 30 min. The lysate was centrifuged at 4°C for 10 min. A bicinchoninic acid protein assay kit was used to measure protein concentration. Protein samples were separated by 10% SDS polyacrylamide gel electrophoresis and electrotransferred to polyvinylidene fluoride (PVDF) membranes. After incubating the cells with BSA blocking solution, the PVDF membrane and primary antibody were incubated overnight at 4°C. The primary antibodies included CD31 (Affinity, 1:1000), VEGF (Affinity, 1:1000), HIF-1α (Affinity, 1:1000), vimentin (Affinity, 1:1000), MMP2 (Affinity, 1:1000), MMP9 (Affinity, 1:1000), and β-actin (Affinity, 1: 4000). The PVDF membrane was incubated with HRP-conjugated goat anti-rabbit secondary antibody (Invitrogen,1:5000). Finally, the protein was visualized by enhanced chemiluminescence and analyzed using ImageJ software.

Cell viability experiment

The MTT colorimetric assay was used to determine the effect of ImP on the viability of cells. The cells (1×10^4 cells/well) were inoculated into a 96-well plate for overnight culture. The experimental group was treated with different concentrations of ImP, and the negative control group was treated with a vehicle control for 48 h. Then, MTT was added to the cells and incubated for 4 h. The formazan crystals were dissolved with 100 μL of DMSO, and the absorbance was measured at 570 nm. The IC_{50} of ImP was calculated using GraphPad Prism 7.0.

Transwell migration assay

Transwell experiment was used to detect the cell migration ability. In the individual culture group, NIH-3T3, HaCaT, and HUVEC cells suspensions were inoculated into the upper chamber of the Transwell chamber separately, and DMEM containing 10% FBS was added to the bottom chamber. In the coculture group, NIH-3T3 or HaCaT cells were seeded to the upper chamber, HUVEC cells were seeded to the lower chamber, and the medium containing different concentrations of ImP was added to the lower chamber. We usually add around 40,000 cells mixed with 200 μL of blank medium into the upper chamber of the Transwell and subsequently incubate for 24-48 h to observe the cell migration. After the experiment, the cells that migrated to the lower part of the Transwell chamber were fixed with 4% paraformaldehyde and stained with 0.1% crystal violet. After the cells on the upper part of the Transwell chamber were gently removed, the migrated cells under a microscope were counted.

Internal cell permeability test

Endothelial cell permeability was assayed using a Transwell chamber. After HUVEC cells were digested, centrifuged, and resuspended, 200 μL of cell suspension containing approximately 40,000 cells is inoculated into the upper chamber of the Matrigel capsule transwell chamber and incubated until the cells are highly integrated. Approximately 500 μL of Incomplete Medium was then added to the lower chamber of the

24-well plate, and TRITC-dextran was added to the upper chamber of the transwell. The liquid from the lower chamber of the 24-well plate was added to the 96-well plate at 100 μL per well, and the fluorescence value was measured using the Infinite M1000 Pro Full Wavelength Multi-Functional Acidic Labeling, which is directly proportional to the permeability of the cells.

Wound healing assay

NIH-3T3, HaCaT, and HUVEC cells were seeded into a 24-well plate, and the experiment was performed after the cell density reached 70%–80% confluence. A scratch was made in the center of each well with a pipette tip. In the coculture group, HUVEC cells (2×10^3 cells/well) were seeded on the upper part of the Transwell chamber with a pore size of 3 μm. NIH-3T3 or HaCaT cells were seeded into a 24-well plate (2×10^5 cells/well), and the Transwell chamber was placed in the 24-well plate to ensure that the liquid was circulating. ImP was diluted in an FBS-free medium and added to the HUVEC cells. The distance of the wound was photographed at 0 and 24 h with an optical microscope. Three biological replicates were set in each group.

Immunofluorescence

Immunofluorescence was used to localize the protein of interest in the cells. Cells in good growth condition were inoculated into 24-well culture plates attached to cell climbing sheets and treated with different drugs. At the end of the treatment the cells were first fixed with 4% paraformaldehyde for 20 min at room temperature and then the wells were closed and punched with closed punch solution for 30 min. After that the cells were sequentially incubated with the corresponding primary and secondary antibodies and blocked with DAPI. Finally, they were observed under a confocal microscope.

qPCR

Total RNA was first extracted from the treated cell samples and the relevant concentrations were determined. The RNA was then reverse transcribed to cDNA using an SYBR RT PCR kit and specific primers. Finally, the expression level was quantified using the $2^{-\Delta\Delta}$Ct method. Graphs were created using GraphPad Prism.

Proteomics analysis

The cells treated with S1P or ImP were collected, and the proteins in the cell lysates were identified by mass spectrometry seperatly. The differentially expressed proteins (|logFC| > 1.5) were analyzed by Gene Ontology (GO) and KEGG analysis to detect S1P- or ImP-induced changes in molecular functions, biological processes, and cellular components. The String database (STRING) (https://string-db.org) was used to analyze the protein–protein interactions network.

Animal experiments

Establishment of T2DM skin wound model

After the mice were adaptively reared for 3–5 days, they were fed with high-fat diet (basic feed mixed with sucrose, lard, and fresh eggs; 15%–18% protein, 51%–54% carbohydrate, 22%–25% fat, and 20.08 kJ/g calories) for 4 weeks. On the first and sixth days of the 11-week-old mice, the mice were fasted overnight and then intraperitoneally injected with low-dose Streptozotocin (STZ). At the end of 12 weeks, the mice were monitored for fasting serum glucose (FSG), and mice with FSG higher than 16.7 mmol/L were selected as the high-fat diet–induced type 2 diabetes model (HFD-T2DM) mice for subsequent experiments. One part was used to establish skin wound models, and one part was used to establish pseudo germ-free (PGF) mice models. To establish the wound model, a hole punch was used to make a 6 mm diameter wound on the skin of the mouse's back. Each group included six mice. On the second day, mice in the control group were coated with 2.5% carboxymethyl cellulose gel. Carboxymethyl cellulose gel containing ImP was applied to the wounds of the mice. Wound length and width were measured daily with vernier calipers, and wound area was calculated. On the ninth day of the experiment, the skin tissue of the wound was collected after anesthesia for the follow-up pathological experiment. According to the formula relative wound area = (1 − current wound area/original wound area) × 100%, and the wound healing rate was calculated. Fontana–Masson staining and hematoxylin–eosin (H&E) staining were used to evaluate the pathological changes of the skin tissues. The normal mice skin wound model were also established and treatment with ImP according to the above method.

Establishment of PGF mice skin wound model

HFD-T2DM mice was selected, and each group included six mice. First, the mice received amphotericin B (1 mg/kg) gavage treatment for 3 days to inhibit the growth of fungi. From the third day, 1 mg/mL ampicillin (A) was added to drinking water. A mixture of antibiotics, including vancomycin (50 mg/kg), neomycin (100 mg/kg), metronidazole (100 mg/kg) and amphotericin-B (1 mg/kg) was administered to the mice through gavage for 12 h. The procedure was continued for 24 days to establish an antibiotic-induced PGF-T2DM model. After making the wound, the mice were injected with ImP by intragastric administration (simulating the process of ImP entering peripheral blood from the digestive system), and wound healing rate was observed and recorded as the T2DM skin wound model.

Sampling process of skin wound

After local scabs appeared in the mouse skin wound model, sterilized cotton swabs were dipped into the sterilized 1× PBS, and the wound was gently scraped without blood. Then, the cotton swabs were immediately transferred to sterilized centrifuge tubes, which were placed on ice and then transferred to a refrigerator for storage at −80°C. Subsequent 16S rRNA sequencing and preliminary analysis were commissioned by Crystal Energy Biotechnology Co., Ltd. (Shanghai, China).

Spns2$^{-/-}$ mice identification

The offspring mice were obtained, and the toes of the offspring mice were clipped with sterilized surgical scissors. The toes were placed in sterile EP tubes placed on ice and then transferred to the refrigerator (−80°C) and stored for homozygous gene detection. Spns2 gene knockout homozygous mice (Spns2$^{-/-}$) were selected and identified for subsequent experiments.

16 S rRNA sequencing and functional analysis

Normal mice were randomly divided into cages and kept for 1 week to normalize the intestinal microbiota prior to the establishment of the T2DM model.The intestinal microbiota in the feces of mice in the normal, model, and HMPA (15 mg/kg)-treated groups were analyzed by Genergy Biotechnology using 16S rRNA sequencing ($n = 6$). Group size was determined using G*Power software based on the effect size of 4.89 (calculated as the ratio of bacillus-like to fungal change), $\alpha = 0.05$, and $1 - \beta = 0.80$ from the preliminary experiments, and the results showed that $n \geq 6$. The PICRUST software package 1.1.3 was used to predict the intestinal microbiota based on the sequences of the 16S rRNA-tagged genes and functional profiles. An interspecies co-abundance network analysis was performed based on Spearman correlation. Only connections with ρ values greater than 0.6 or less than −0.6 were used for network construction and visualization. For network construction and visualization based on Cytoscape software.

Immunohistochemistry

The expression of vimentin, VEGF, CD31, Ki67, and other proteins in the skin tissues of the wounds was assayed by immunohistochemical experiments. The tissue sections were deparaffinized and hydrated, and then antigen retrieval was performed with 0.01 M citrate buffer. After blocking with serum for 30 min, the slide was placed in a humidified box and incubated with the primary antibody overnight. After the primary antibody was washed off, a sensitizer was added, and the sections were incubated for 20 min. Then, biotinylated goat anti-rabbit secondary antibody was added for 30 min of reaction. Finally, the slides were stained with DAB and hematoxylin, observed under a microscope, and photographed. The staining intensity was scored as follows: none (0), light brown (1+), medium brown (2+), and dark brown (3+). According to the percentage of stained skin cells, the percentage of positive cells was divided into four grades, that is, 1 (1%–25%), 2 (25%–50%), 3 (50%–75%), and 4 (>75%).

QUANTIFICATION AND STATISTICAL ANALYSIS

The statistical analyses were performed using GraphPad Prism version 7. Statistically significant differences were calculated using two-tailed unpaired t-tests or unpaired t-test with Welch's correction, Pearson's correlation, and Kaplan–Meier. Data were presented as mean ± standard deviation (SD). The significance criteria were as follows: *$p < 0.05$ and **$p < 0.01$.